Secondary Irregularities in the Equatorial Electrojet

Short title: (Secondary equatorial-electrojet irregularities)

Robert Cohen and Kenneth L. Bowles*

Institute for Telecommunication Sciences and Aeronomy**

Environmental Science Services Administration, Boulder, Colorado

ABSTRACT

Although the two-stream instability theory [Farley, 1963a,b] has been quite successful in accounting for many observed features of the plasma-wave irregularities produced in the equatorial electrojet, increased equipmental sensitivity and improved experimental techniques of observing the power spectrum of radio echoes from the electrojet have resulted in the resolution of weaker irregularities not predicted by that theory. In particular, such irregularities are observed both when a VHF radar located near the magnetic equator is directed vertically, and when the radar is directed obliquely in the equatorial plane. In the latter case, the irregularities have lower Doppler shifts than are suggested by the theory. Experimental spectra are presented that demonstrate features consistent with the first-order two-stream theory for observations of a well-developed electrojet at oblique angles of incidence. However, the relative contribution of the weaker irregularities can be resolved in spectra for incidence angles approaching the zenith or, when the electrojet is comparatively weak, at most angles. The spectral width obtained at vertical incidence is shown to be narrow for a weak electrojet, and to be broadened as the electrojet becomes stronger. The weaker irregularities probably result from the non-linear interaction among the stronger irregularities, as is demonstrated by Dougherty and Farley [1966] in a companion paper. Experimental results are presented that indicate and asymmetry not predicted by either theory; i.e., the upgoing irregularities (observed at angles of incidence west of the zenith) are stronger than the downgoing irregularities (observed at angles of incidence east of the zenith). This

---

*Now at Department of Applied Electrophysics, University of California at San Diego, La Jolla, California.

**Formerly Central Radio Propagation Laboratory, National Bureau of Standards.

asymmetry may be accounted for by the variation with height of the physical properities of the region of instability.

KEY WORDS: Irregularities
Equatorial electrojet
Plasma instability
Two-stream instability
Plasma waves
Ion-acoustic waves
Non-linear coupling
Ionosphere
Ionospheric irregularities
Equatorial ionosphere
Equatorial E region

Secondary Irregularities in the Equatorial Electrojet

Short title: (Secondary equatorial-electrojet irregularities)

Robert Cohen and Kenneth L. Bowles*
Institute for Telecommunication Sciences and Aeronomy**
Environmental Science Services Administration, Boulder, Colorado

1. Introduction

The characteristics of electron density irregularities in the equatorial electrojet have been studied experimentally by means of trans-equatorial VHF forward scattering [Bowles and Cohen, 1962; Cohen and Bowles, 1963a,b], standard ionograms [Cohen et al., 1962], and VHF radar [Bowles et al., 1960, 1963; Balsley, 1965]. A theoretical explanation of the origin of such irregularities has been presented by Farley [1963a,b], who attributed electron-density fluctuations to ion-acoustic waves associated with the two-stream plasma instability. The principal features of the experimental observations were accounted for by that theory, but certain questions regarding additional features have remained to be answered.

One such question concerned the mechanism for the production of irregularities with horizontal wave fronts. These irregularities are clearly associated with the equatorial electrojet [Cohen and Bowles, 1963a], but are not predicted by Farley's theory. They are responsible for the daytime equatorial VHF forward scatter and for radar echoes obtained from the electrojet at vertical incidence.

Another question was raised by the unexplained observation of certain electrojet irregularities moving at speeds slower than the acoustic velocities predicted by the theory. Such motions were noted [Bowles et al., 1963] on spectra of VHF radar echoes from the electrojet.

These difficulties of the first-order theory were recognized [Bowles et al., 1963; Cohen and Bowles, 1963a; Farley, 1963b], and Farley [1963b] hypothesized that the probable explanation was non-linear coupling among the first-order plasma waves. In a companion paper, Dougherty and Farley [1966] present a detailed treatment of how this non-linear coupling gives

---

*Now at Department of Applied Electrophysics, University of California at San Diego, La Jolla, California.

**Formerly Central Radio Propagation Laboratory, National Bureau of Standards.

rise to secondary irregularities and to the observed spectra.

Although previously published experimental spectra have provided some evidence about the characteristics of the secondary electrojet irregularities, improved instrumentation has meanwhile enabled the acquisition of high-resolution spectra, which aid considerably in elucidating the phenomena under discussion. The present paper reviews the latest experimental knowledge on this subject and defines areas of agreement and residual points of disagreement between available theory and experiment.

2. Technique

Considerable improvement in instrumentation has been effected since the previous publication [Bowles and Cohen, 1962; Bowles et al., 1963a] of spectra of VHF echoes from electrojet irregularities. Besides the greater sensitivity available at the Jicamarca Radar Observatory*(11.95°S, 76.87°W; dip: 2°N), associated with the availability of high-power transmitters and rotatable mattress-antennas capable of handling such power, there has also been a fundamental improvement resulting from employing an autocorrelation analysis of the received signal instead of a panoramic spectrum analysis. This procedure is preferable from an information-theory standpoint.

The autocorrelation functions obtained in the recent measurements are Fourier-transformed to the associated spectra by use of a computer program. The autocorrelation function is obtained in the following manner: A series of transmitted pulses is emitted, each pulse having an amplitude proportional to $\mathrm{Re}\left\{\exp(i\omega_o t)\right\}$, where ω_o is the angular frequency of the transmitter. The signal entering the receiving antenna is proportional to $\mathrm{Re}\left\{a(t)\exp\left(i[\omega_o t - \varphi(t)]\right)\right\}$. A synchronous demodulator is used to mix the received signals to baseband at the receiver output, and has the effect of implementing the following equations:

$$A(t) = \mathrm{Re}\left\{a(t)\exp i[\omega_o t - \varphi(t)]\,\exp(-i\omega_o t)\right\} = a(t)\cos[\varphi(t)]$$

$$B(t) = \mathrm{Re}\left\{a(t)\exp i[\omega_o t - \varphi(t)]\,\exp[-i(\omega_o t - \pi/2)]\right\} = a(t)\sin[\varphi(t)].$$

A(t) and B(t) are separately available at the output terminals of the syn-

*A cooperative project of the Institute for Telecommunication Sciences and Aeronomy, ESSA, Boulder, Colorado and the Instituto Geofísico del Perú, Lima, Peru.

chronous demodulator. These quadrature outputs are digitized for selected times corresponding to desired radar ranges (the outputs are said to be "range-gated"). Signal levels for one of the channels, A(t), are successively stored in a 64-location memory at intervals of one pulse-repetition period. Appropriate product functions can then be formed in a digital multiplier for obtaining the complex autocorrelation function of the received signal. For each instantaneous pair of samples, A(t) and B(t), product functions are formed as follows: $A(t)A(t - \tau)$ and $B(t)A(t - \tau)$ for each time-delay, τ, where τ varies from 0 to 63 times the pulse-repetition period, T. The newest sample of A(t) then replaces the oldest sample of A(t) in the memory, and the cycle continues.

The normalized autocorrelation function, $\rho(\tau)$, is defined as follows:

$$\rho(\tau) = \frac{\int_{-\infty}^{\infty} S^*(t)\, S(t + \tau)dt}{\int_{-\infty}^{\infty} |S(t)|^2 dt},$$

where in this case S(t) is the complex, range-gated digitized output of the synchronous demodulator, given by $S(t) = A(t) + i\, B(t)$.

Upon replacing S(t) in the expression for $\rho(\tau)$ by this equivalent, we obtain on expanding,

$$\rho(\tau) = \frac{\int_{-\infty}^{\infty} A(t)A(t + \tau)dt + \int_{-\infty}^{\infty} B(t)B(t + \tau)dt + i \int_{-\infty}^{\infty} B(t + \tau)A(t) - i \int_{-\infty}^{\infty} B(t)A(t + \tau)d}{\int_{-\infty}^{\infty} A^2(t)dt + \int_{-\infty}^{\infty} B^2(t)dt}$$

If channels A and B of the synchronous demodulator are precisely matched in gain, it follows that

$$\int_{-\infty}^{\infty} A^2(t)dt = \int_{-\infty}^{\infty} B^2(t)dt.$$

In practice, symmetrization of the channels is achieved on an average basis by interchanging their rôles each time the transmitter is pulsed.

This is accomplished by introducing a 90° phase shift into the input of one of the channels during alternate pulse cycles.

Furthermore, since A(t) and B(t) are stationary random variables obeying the same Maxwellian statistics,

$$\int_{-\infty}^{\infty} A(t)\, A(t+\tau)dt = \int_{-\infty}^{\infty} B(t)\, B(t+\tau)dt, \text{ and}$$

$$\int_{-\infty}^{\infty} B(t+\tau)\, A(t)dt = -\int_{-\infty}^{\infty} B(t)\, A(t+\tau)dt.$$

Accordingly, the expression for $\rho(\tau)$ simplifies to

$$\rho(\tau) = \frac{\int_{-\infty}^{\infty} A(t)A(t+\tau)dt - i\int_{-\infty}^{\infty} B(t)A(t+\tau)dt}{\int_{-\infty}^{\infty} A^2(t)dt}.$$

Since the autocorrelation is a Hermitian function, $\rho(\tau) = \rho^*(-\tau)$, so

$$\rho(\tau) = \frac{\int_{-\infty}^{\infty} A(t)\, A(t-\tau)dt + i\int_{-\infty}^{\infty} B(t)\, A(t-\tau)dt}{\int_{-\infty}^{\infty} A^2(t)dt}.$$

The product-function terms appearing in this integral are those previously referred to as having been formed in a digital multiplier. Assuming that during periods of a few minutes the observed time series is stationary, the infinite integrations are replaced by finite sums over some 10,000 samples of S(t), and the product-terms for each of 64 τ's are integrated in a core memory. This procedure yields 64 pairs of real and imaginary values of the complex autocorrelation function, each pair corresponding to an evaluation of $\rho(\tau)$ for a τ in the interval $0 \leq \tau \leq 63T$, where T is the pulse-repetition period.

The Wiener-Khintchine Theorem states that the signal power spectrum is the Fourier transform of its autocorrelation function, or

$$P(f) = \int_{-\infty}^{\infty} \rho(\tau) e^{-i\,2\pi f\tau}\, d\tau.$$

The integral in this case is replaced by a Fourier sum of sine and cosine terms extending over the discrete values employed for τ. This sum is formed in a computer, employing the measured values of the auto-correlation function, and results in a graph of the power spectrum for frequencies separated from the carrier frequency by as much as $\pm$ 1/2T. This limiting frequency is the 63rd harmonic of the fundamental frequency, 1/2(63T), which is the low-frequency limit of resolution. Points are calculated for each harmonic, and intermediate points interpolated. Insofar as the pulse-repetition period is selected so as to be short enough to sample at a rate more than twice as great as the highest Doppler frequency component, the procedure outlined will provide a good representation of the power spectrum of a signal.

Normalization of each power spectrum plotted in this paper has been accomplished by dividing by the highest value attained by P(f), which thus defines unity on the axis of ordinates. The total integral under the spectrum is given by $\rho(0)$, and this value can be printed by the computer upon request.

The power spectra presented here characterize the instantaneous echo obtained from a portion of the electrojet defined in part by the pulse-width transmitted, the antenna beamwidth and by range-gating of the received signal. Furthermore, the electrojet is of finite thickness, comparable to the 100 μs pulse width used in these experiments (a 100 μs pulse corresponds to 15 km radar-range), and of considerable extent north and south. However, the field-aligned electrojet irregularities restrict electrojet echoes to the nearly vertical east-west equatorial plane because of the phase-coherence or "aspect-sensitivity" requirement. The mattress antennas employed in the experiments described herein were mounted so as to rotate in the equatorial plane, and their half-power beamwidth in that plane was about 35°. Range-gating was employed to

select echoes of delays appropriate to the height of the electrojet and corresponding to the nominal direction of the antenna. As is apparent from the sketches of Figure 1, the range-gating technique provides a considerable improvement over the spatial resolution otherwise obtainable with antenna-beams this wide. FIG. 1

Some of the figures presented in this paper indicate the variation of the power spectrum as a function of the eastward angle from the vertical, θ. There is a tacit assumption in such experimentation somewhat analogous to an ergodic hypothesis; namely, that the essentially simultaneous study of various spatial regions of the electrojet from one vantage point and at various angles is equivalent to studying the same spatial region (with various radars) from several vantage points. Either procedure would yield a spectral dependence on θ, but it is obviously more feasible to study the electrojet irregularities with but a single radar, and it is apparent that the electrojet is sufficiently homogeneous to permit this. Using narrow pulses, Balsley [1965] has identified east-west structure in the electrojet. Such structure would not complicate the interpretations in the present treatment, nor presumably would the east-west asymmetry discussed in a later section.

3. Recapitulation of spectral results for the primary irregularities

By employing the improved instrumentation described in the previous section, a number of power spectra have been obtained at the Jicamarca Radar Observatory during January, 1964 for echoes from equatorial electrojet irregularities under various conditions. The frequency of observation was usually 49.92 Mc/s, although some measurements were made using 147.76 Mc/s and several frequencies below 10 Mc/s.

A composite of such power spectra during times when the electrojet was relatively strong is shown in Figure 1, illustrating the nearly identical Doppler shifts obtained for appreciably different angles, θ, from the vertical, as predicted by the two-stream instability theory of Farley [1963b]. On observing east of the vertical, a positive Doppler shift corresponding to a downward motion of irregularities is obtained,

while on observing west of the vertical, there is a negative Doppler shift corresponding to an upward motion of irregularities.

The selection of downward or upward moving irregularities as a function of the direction of observation is illustrated in Figure 2. The propagation vector, $\underline{k}$, is directed at angle β from the vertical. Because of the "aspect sensitivity" of reflection, echoes can be obtained only from those plane-wave irregularities with wavefronts moving along $\underline{k}$. Consequently, on observing toward the east ($\beta > 0^{\circ}$), irregularities moving downward at an angle ($90^{\circ} - |\beta|$) are detected, while on observing toward the west ($\beta > 0^{\circ}$), irregularities moving upward at that angle are detected. A typical angular aperture in which primary irregularities are present at a given time is shown at the center of the diagram as having a half-width θ. Ion-acoustic waves of identical phase velocity emanate in all westward directions within that aperture.

FIG. 2

At the frequency of observation, 49.92 Mc/s, a frequency-shift of 100 c/s corresponds to a velocity of 300 m/s, so the shifts of about $\pm$ 140 c/s shown in Figure 1 for $\beta = \pm 70^{\circ}$ and $\beta = \pm 45^{\circ}$ are associated with a phase velocity toward or away from the radar of about 420 m/s.

According to the calculations of Farley [1963b], the observed phase velocity at this frequency should exceed the ion-acoustic velocity in the medium by about 7%, assuming an infinite growth time. The measurements in Figure 1 would thus imply an ion-acoustic velocity of 390 m/s. The ion-acoustic velocity, v_i, is given by $(2RT/m_i)^{\frac{1}{2}}$, where R is the universal gas constant, T is the absolute gas temperature, and m_i is the mean molecular weight of the ions. Assuming that the mean height of the electrojet is 105 km, and employing the atmospheric model of Champion and Minzner [1963], m_i at this height is estimated at 28.72. The temperature at this height may then be derived from a rearrangement of the above relation; i.e., $T = v_i^2 m_i/2R$. This gives a calculated value for T of 265°K, using $v_i = 390$ m/s. The Champion and Minzner model would predict about 235°K at 105 km. The fact that electrojet irregularities are observed most of the day for ion-acoustic velocities in this range implies that the average electron drift velocities usually exceed these values. Consequently, the average electron

drift velocity of 2.7 km/s obtained for the electrojet model of Sugiura and Cain [1966] seems more appropriate than the value 310 m/s for Zmuda's model [1960].

The above discussion relates the experimental results of Figure 1 with predictions of the first-order two-stream instability theory. Spectra illustrating another feature predicted by the theory are now available; they refer to the relative phase velocity of the ion waves of various wavelengths as observed at different frequencies. By observing nearly simultaneously at several frequencies, such as at 49.92 and 147.76 Mc/s, echoes can be obtained corresponding to irregularity wavelengths of about 3 and 1 meters, respectively. An example of such an observation is shown in Figure 3. Since the ratio of frequencies is nearly 3:1 (2.96), the common frequency-shift axis employed is scaled by a factor of 3 for the purpose of readily comparing the two measurements. If the same irregularities were being observed at each frequency, or if all irregularities were moving at the same velocity, then the corresponding Doppler shifts would be scaled by the frequency ratio. However, as predicted by the theory [Farley, 1963b], this is not the case, and there is a larger relative frequency shift at the higher frequency. The actual frequency shifts obtained in this case were about 97 c/s and 323 c/s, which are in the ratio 1.12 to 1 when corrected for the frequency ratio. This is comparable to the ratio of about 1.10 to 1 predicted from Figure 7 of Farley's paper, using an infinite growth time.

FIG. 3

4. Spectral characteristics of the secondary irregularities

The power spectra of electrojet echoes can show appreciable variation from those of Figure 1, which are characteristic of a strong electrojet. That is, they vary in form with the strength of the electrojet and also with the angle of observation, β. The first-order theory [Farley, 1963 a,b] would predict plane wave irregularities at large and intermediate angles, and no irregularities at small angles. That theory would also predict that the echo spectrum should not vary with angle, except to be reflected in the axis of ordinates when β changes sign, with the echo disappearing completely as β approaches zero. Even in Figure 1 one can note discre-

pancies with the first-order theory, in that at $\pm 45^{\circ}$ there is an appreciable amount of echo at frequency-shifts differing from the preponderant ± 140 c/s. Also, there is considerable echo at vertical incidence ($\beta = 0^{\circ}$), indicating the presence of irregularities with horizontal wave fronts moving upward and downward at substantial velocities. The comparative integrated echo-powers of the spectra of Figure 1 at angles $\beta = 0^{\circ}$, $\pm 45^{\circ}$ and $\pm 70^{\circ}$ are not obtainable from that figure. The angular dependence of integrated echo-power when corrected for the radar sensitivity is shown (for a similar measurement) in Figure 3 of Bowles et al [1963].

The secondary irregularities probably do not originate from the "wind-shear" mechanism associated with "Sporadic E" irregularities at other latitudes, since that process is not operative near the magnetic equator [Axford and Cunnold, 1966]. Furthermore, neither equatorial ionogram configurations [Knecht and McDuffie, 1962] nor equatorial VHF forward scatter propagation [Bowles and Cohen, 1962; Cohen and Bowles, 1963b] show evidence of the presence of temperate latitude Sporadic E irregularities.

The behavior of the power spectrum of radar echoes at vertical incidence as a function of the electrojet strength is shown in Figure 4. A set of four vertical-incidence power spectra (including that of Figure 1) are superimposed, corresponding to the total magnetic field strengths measured at the times shown by the arrows. Since the magnetic field at Jicamarca is essentially horizontal, the total field as measured by a rubidium-vapor magnetometer is a close approximation to the horizontal field. However, the horizontal field variation is not entirely controlled by the variations of the electrojet current, but also by currents outside the electrojet [Cohen and Bowles, 1963a]. That may explain why the spectrum at 1158 is broader than that at 1108, even though the total field at those times was nearly the same. This is because the apparent strength of the electrojet in the morning, based on geomagnetic field measurements at the earth's surface, seems to be higher than its actual strength, due to an additive current elsewhere; and lower in the afternoon, because of a current in the opposite sense. (This explanation would also account

FIG 4

for the tendency of the horizontal field at the equator to attain a maximum before noon, rather than the noontime maximum associated with the electrojet variation.)

We conclude from Figure 4 that the stronger the electrojet, the broader the spectrum obtained at vertical incidence. There is no appreciable displacement of the central frequencies from the carrier frequency, but there does seem to be a slight preference for negative shifts of about 100 c/s compared to positive shifts of that amount; i.e., there is a slight asymmetry favoring upward motions as compared to downward motions, especially noticeable in the spectrum of 1158. There will be further discussion of this asymmetry in the following section of this paper. But for the slight asymmetry, the observed behavior with electrojet strength is what would be predicted by the non-linear coupling theory of Dougherty and Farley [1966], since on that theory the relative amount of secondary irregularities having appreciable upward or downward velocities would be expected to increase with the electrojet strength.

It is interesting to relate the observations of Figure 4 with some earlier experiments. During the International Geophysical Year period, frequency variations were noted on VHF forward scatter signals propagated by the equatorial electrojet [Cohen and Bowles, 1963b]. In that study, it was found that the bandwidth of the propagation, as measured by the 'fading rate', was closely related to the strength of the electrojet, as was the signal intensity. This is illustrated in Figure 5, which is reproduced from Cohen and Bowles [1963a]. The south → north oblique scatter propagation at 50 Mc/s resulted from vertically-moving secondary irregularities in the electrojet. The IGY observations were somewhat equivalent to what would have been obtained by a radar at vertical incidence ($\vartheta = 0^{\circ}$) employing a frequency about 20% as great, near 10 Mc/s. Thus the fading frequencies of Figure 5 are only about one-fifth the average frequencies of Figure 4.

FIG 5

The fading rate measurement of Figure 5 was obtained by an instrument that counted the relative number of crossings of a reference value of the signal, and is closely related to the effective bandwidth of the signal. A scatter-plot of values of fading rate vs. signal strength from

Figure 5 implies a correlation between these variables of about 0.9, following the correlogram analysis of Sugar [1954]. Such a high correlation would be expected, since each of the variables has been separately demonstrated to correlate with the magnetic field strength. However, either variable is perhaps a better absolute measure of the electrojet strength than is the magnetic field strength.

Another variation with electrojet strength of the power spectrum of radar echoes from the electrojet is shown in Figure 6, this time at an angle of $\beta = 50^{\circ}$. Here the predictions of the secondary-irregularity theory of Dougherty and Farley [1966] are well illustrated. For a weak electrojet, at 1010, the spectrum maximizes at a frequency well below the acoustic velocity, but as the electrojet builds up, such as at 1049, the plasma-wave peak becomes manifest. As the electrojet becomes stronger, at 1105, the plasma wave irregularities predominate even more over the secondary irregularities, until at 1129 there is no longer the secondary maximum at low frequencies that was apparent earlier, although there are still a large number of secondary irregularities present.

FIG. 6

We have just noted in Figure 6 the variation of spectrum with electrojet strength at a constant angle of incidence. It is also interesting to study the variation of the power spectrum with angle for a fairly large but nearly constant value of electrojet strength. This is shown in Figure 7 for angles of 60°, 45°, 30° and an angle less than 30°. It is apparent that the relative strength of the plasma wave irregularities compared to the secondary irregularities is changing with angle in the detailed way that would be expected from the theory. That is, the strength of the secondary irregularities should predominate over that of the primary irregularities at small values of β, but be of decreasing importance compared to the plasma waves as β approaches large values.

FIG. 7

5. Asymmetry of the upgoing and downgoing irregularities

As noted in the preceding section in connection with the vertical incidence observation of Figure 4, there is an asymmetry in strength of the upward-going vs. the downward-going irregularities, in that the former

tend to be somewhat stronger. This is particularly apparent for non-zero values of β at times when the electrojet is stable and of intermediate strength, as for the examples shown in Figures 8 and 9, for $\beta = \pm 50^{\circ}$. These figures represent a superposition of spectra for three sequential times, with a spectrum at $\beta = +50^{\circ}$ preceding and following a spectrum for $\beta = -50^{\circ}$. This "sandwich" technique thus establishes the validity of a comparison for positive and negative β insofar as time-invariance of electrojet-strength is concerned.

FIG. 8
FIG. 9

In Figure 8, there are scarcely any secondary irregularities apparent looking westward at the upward-moving irregularities, whereas on looking eastward at the downward-moving irregularities, an appreciable admixture of secondary irregularities is noted. However, the westward observations of Figures 8 and 9 should not be interpreted as implying that there are no secondary irregularities present; instead, the inference should be that the primary irregularities are so strong that, as a consequence of the normalization procedure employed, the presence of the secondary irregularities is suppressed. In fact, the numerosity and/or strength of the secondary irregularities viewed toward the west probably exceed(s) the numerosity and/or strength of those observed on looking toward the east. This situation is even more pronounced in Figure 9, where there is little, if any, evidence of plasma waves for the eastward observations. The electrojet corresponding to Figure 9 is somewhat weaker than that for Figure 8. Note that this change in electrojet strength results in an appreciable redistribution of power between the primary and secondary irregularities for the eastward observations, but there is little noticeable effect for the westward observations. These results are not predicted by currently available theory, and are typical of a tendency for westward electrojet echoes to be stronger than those from the east.

It could be conjectured that such results might arise if a stratum at the base of the electrojet were more conducive to the formation of plasma waves than a stratum at the top of the electrojet. This is because the stratum at the base might produce mainly upward-going irregularities, while that at the top might produce mainly downward-going irregularities.

The height region occupied by the equatorial electrojet embraces several scale-heights. This means that the physical characteristics of the ionospheric E region, such as electron concentration, are varying appreciably with height within the electrojet. Consequently, the base and top of an unstable portion of the electrojet would be expected to have significantly different properties for the formation of irregularities. The existence of strata of irregularities in the electrojet has been evidenced by observations of vertical bifurcation and of east-west patchiness [Cohen et al, 1962; Balsley, 1965].

6. Discussion and conclusions

This paper has presented recent spectral observations of echoes from irregularities in the equatorial electrojet. These spectra are of improved definition compared to those previously available, and help resolve certain features of the primary and secondary irregularity structure of the plasma waves. General agreement with theory has been obtained, although there is an as yet unexplained tendency for asymmetry in the nature of the irregularities traveling upward compared to those moving downward. Furthermore, details regarding the strength of the irregularities and growth of the instability are not treated by existing theory.

ACKNOWLEDGEMENTS

Computer programming of the Fourier-series transformation was by Donald L. Sterling. Considerable stimulus and helpful discussions were provided by John P. Dougherty and Donald T. Farley, Jr., and by Ben B. Balsley. The experimental collaboration of John L. Green, Antonio Arévalo and Jesús Córdova has been indispensable. Computer data-processing was by Gerardo Vera.

REFERENCES

Axford, W. I. and D. M. Cunnold, The wind-shear theory of temperate zone Sporadic E irregularities, Radio Science, 1, 191-198, 1966.

Balsley, Ben B., Some additional features of radar returns from the equatorial electrojet, JGR, 70, 3175-3182, 1965.

Bowles, K. L., B. B. Balsley and Robert Cohen, Field-aligned E-region irregularities identified with acoustic plasma waves, JGR, 68, 2485-2501, 1963.

Bowles, Kenneth L. and Robert Cohen, A study of radio wave scattering from Sporadic E near the magnetic equator, in Ionospheric Sporadic E, pp. 51-77, edited by E. K. Smith and S. Matsushita, Pergamon Press, London, 1962.

Bowles, K. L., R. Cohen, G. R. Ochs and B. B. Balsley, Radio echoes from field-aligned ionization above the magnetic equator and their resemblance to auroral echoes, JGR, 65, 1853-1855, 1960.

Champion, Kenneth S. W. and Raymond A. Minzner, Revision of United States Standard Atmosphere 90 to 700 kilometers, Rev. Geophys., 1, 57-84, 1963.

Cohen, Robert and Kenneth L. Bowles, The association of plane-wave electron-density irregularities with the equatorial electrojet, JGR, 68, 2503-2525, 1963a.

Cohen, Robert and Kenneth L. Bowles, Ionospheric VHF scattering near the magnetic equator during the International Geophysical Year, J. Res. NBS, 67D, 459-480, 1963b.

Cohen, Robert, Kenneth L. Bowles and Wynne Calvert, On the nature of Equatorial Slant Sporadic E, JGR, 67, 965-972, 1962.

Dougherty, J. P. and D. T. Farley, Ionospheric E-region irregularities produced by non-linear coupling of unstable plasma waves, JGR, 71, (this issue), 1966.

Farley, D. T., Jr., Two-stream plasma instability as a source of irregularities in the ionosphere, Phys. Rev. Letters, 10, 279-282, 1963a.

Farley, D. T., Jr., A plasma instability resulting in field aligned irregularities in the ionosphere, JGR, 68, 6083-6097, 1963b.

Knecht, R. W. and R. E. McDuffie, On the width of the equatorial E_s belt, in Ionospheric Sporadic E, E. K. Smith, Jr. and S. Matsushita, eds., pp. 215-218, (Pergamon Press, London, 1962).

Sugar, George R., Estimation of correlation coefficients from scatter diagrams, J. Applied Physics, 25, 354-357, 1954.

Sugiura, Masahisa and Joseph C. Cain, A model equatorial electrojet, JGR, 71, 1869-1877, 1966.

Zmuda, A. J., Ionospheric electrostatic fields and the equatorial electrojet, JGR, 65, 2247-2253, 1960.

TITLES FOR FIGURES

Figure 1. Composite of power spectra obtained near noon for echoes from electrojet irregularities above Jicamarca, Peru at angles of incidence, β, east of the vertical, of 0°, $\pm 45^{\circ}$ and $\pm 70^{\circ}$. These spectra correspond to a relatively strong electrojet.

Figure 2. Schematic representation of the selection of upward- or downward-moving plasma waves according as the radar beam is directed westward ($\beta < 0^{\circ}$) or eastward ($\beta > 0^{\circ}$), respectively.

Figure 3. Power spectra for echoes from electrojet irregularities obtained nearly simultaneously at several frequencies for an angle of incidence of $\beta = 45^{\circ}$. The vertical dashed lines indicate the net shifts associated with the two observations. The exact frequencies utilized were 49.92 Mc/s and 147.76 Mc/s.

Figure 4. Power spectra for echoes at vertical incidence ($\beta = 0^{\circ}$) from electrojet irregularities, compared with the variation of the total geomagnetic field. The arrows along the time-axis of the magnetic-field graph refer to the times at which the power spectra were obtained.

Figure 5. Field strength and fading rate of a/50 Mc/s signal forward scattered via the equatorial electrojet from Arequipa to Trujillo, Peru on 1958 October 24, compared to the variation of the horizontal component of the geomagnetic field observed at Huancayo, Peru (12.05°S, 75.33°W; Dip: 2°N). Local time is 75°W.

Figure 6. Variation of the power spectrum with changing electrojet strength at a constant angle of incidence ($\beta = 50^{\circ}$), compared with that of the total geomagnetic field. The arrows along the time-axis of the magnetic-field graph refer to the times at which the power spectra were obtained.

Figure 7. Power spectrum for a relatively strong and steady electrojet at various angles of incidence ($\beta = 60^{\circ}$, 45°, 30° and $0^{\circ} < \beta < 30^{\circ}$).

Figure 8. Power spectra at symmetric angles of incidence ($\beta = \pm 50^{\circ}$) for a steady but relatively weak electrojet.

Figure 9. Power spectra at symmetric angles of incidence ($\beta = \pm 50^{\circ}$) for a steady electrojet that is even weaker than that to which Figure 8 corresponds.

JICAMARCA, PERU

1964 JANUARY 3

75°W. LOCAL TIME

f_o = 49.92 Mcs

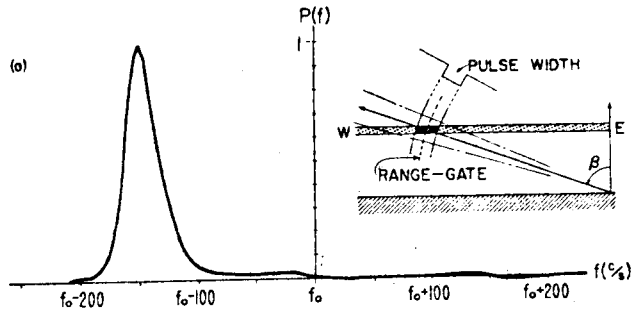

ANTENNA 70° WEST $11^h\ 40^m$

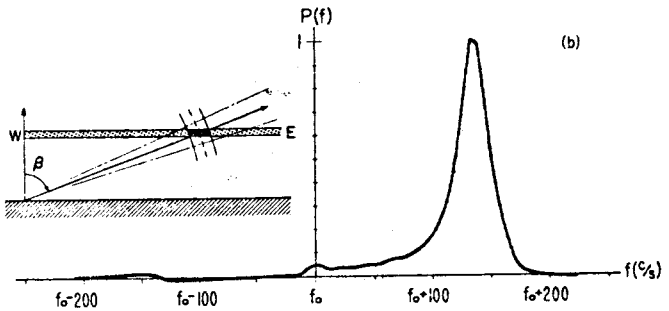

ANTENNA 70° EAST $12^h\ 15^m$

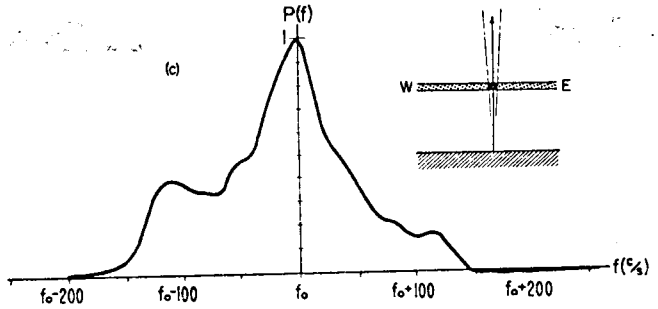

ANTENNA VERTICAL $11^h\ 58^m$

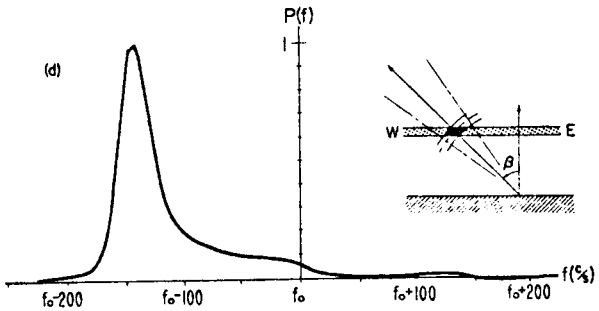

ANTENNA 45° WEST $11^h\ 48^m$

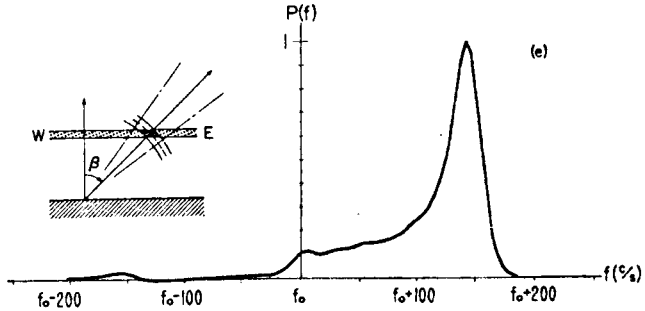

ANTENNA 45° EAST $12^h\ 08^m$

B-61486

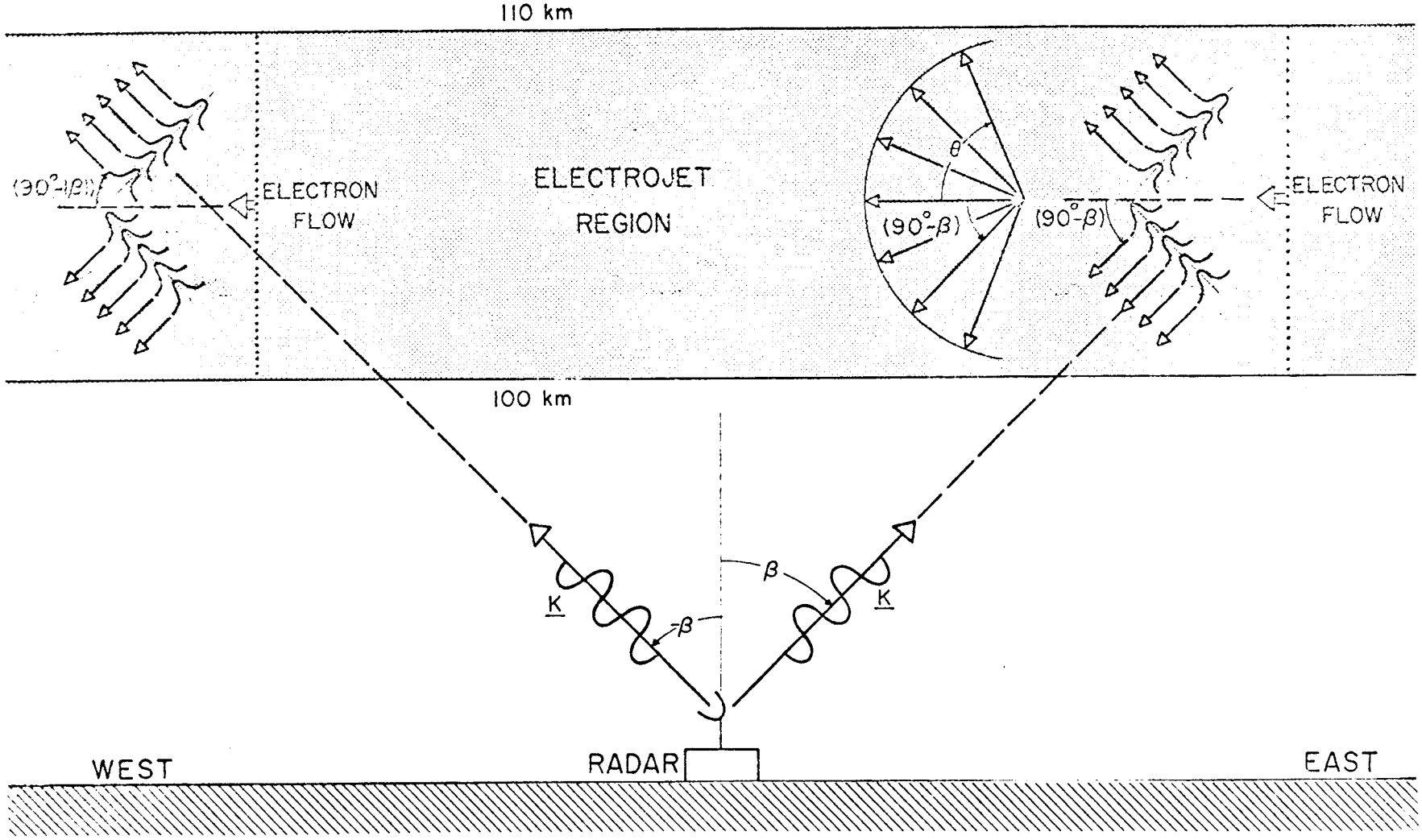
110 km
ELECTRON FLOW
ELECTROJET REGION
θ
(90°-β)
(90°-β)
ELECTRON FLOW
100 km
K
β
β
K
WEST
RADAR
EAST

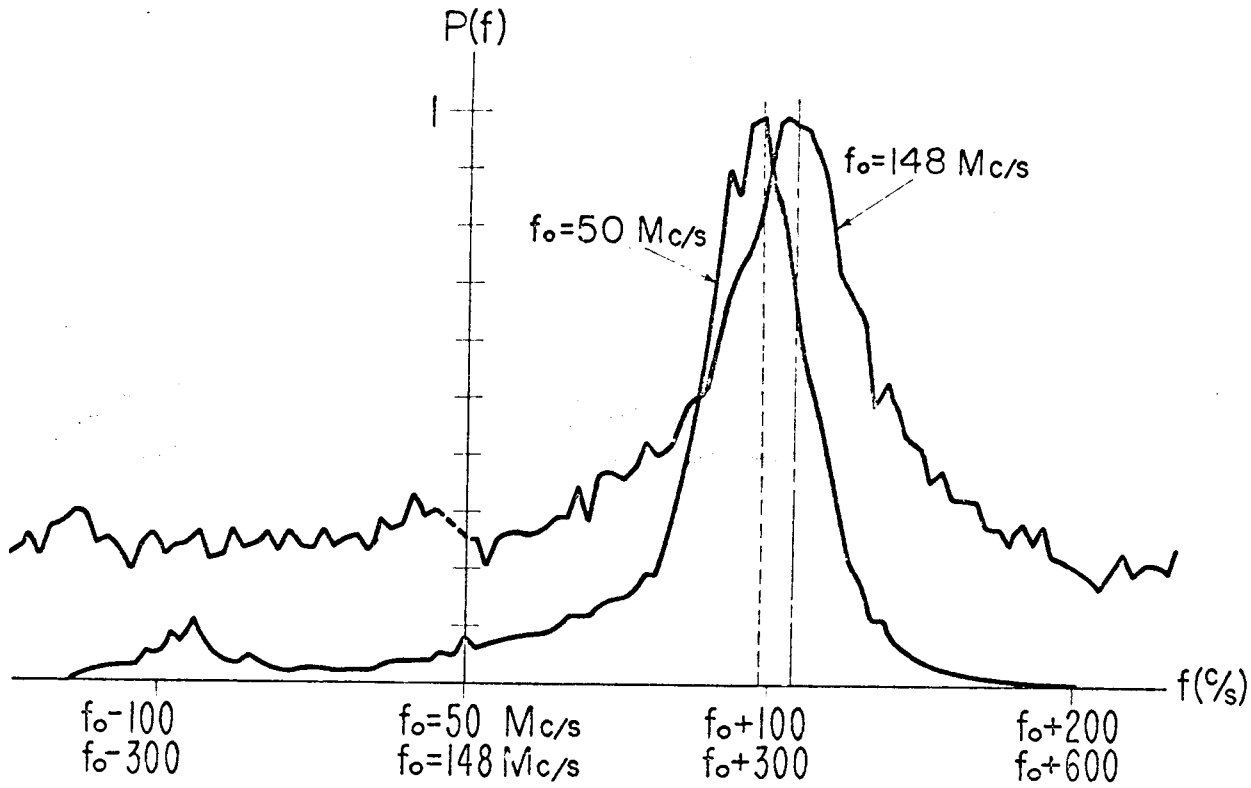

JICAMARCA, PERU
1964 JANUARY 16
75°W. LOCAL TIME

$t_{50\,Mc/s} = 10^h47^m30^s$

$t_{148\,Mc/s} = 10^h40^m30^s$

—45° EAST—

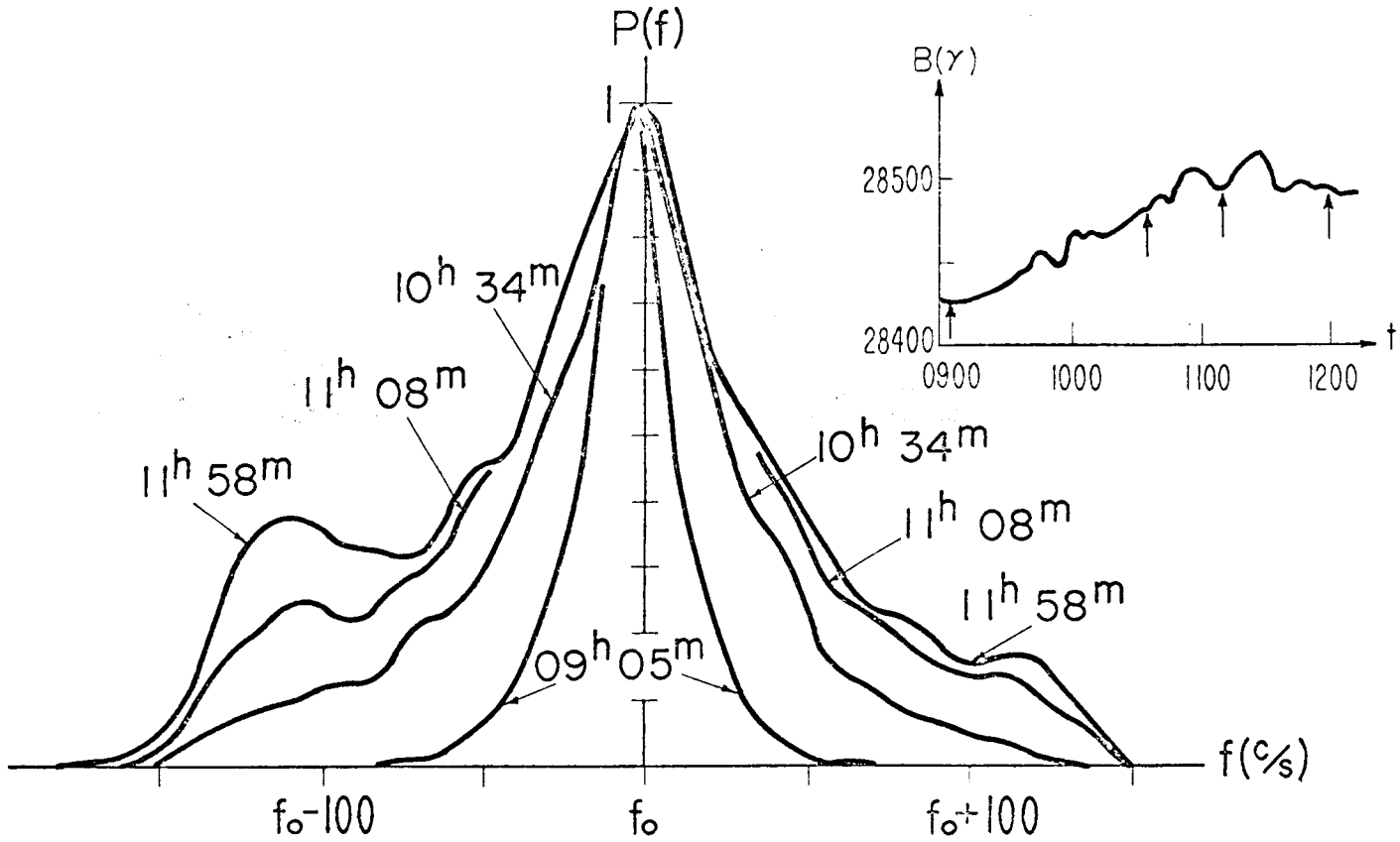

JICAMARCA, PERU
1964 JANUARY 3
75°W. LOCAL TIME
f_o = 49.92 Mc/s
—VERTICAL—

50 Mc/s FADING RATE (AREQUIPA → TRUJILLO)

24 OCTOBER 1958

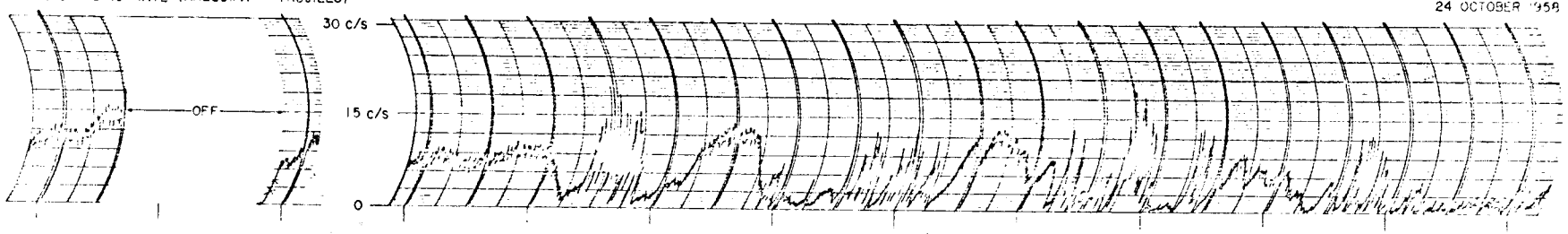

H (HUANCAYO)

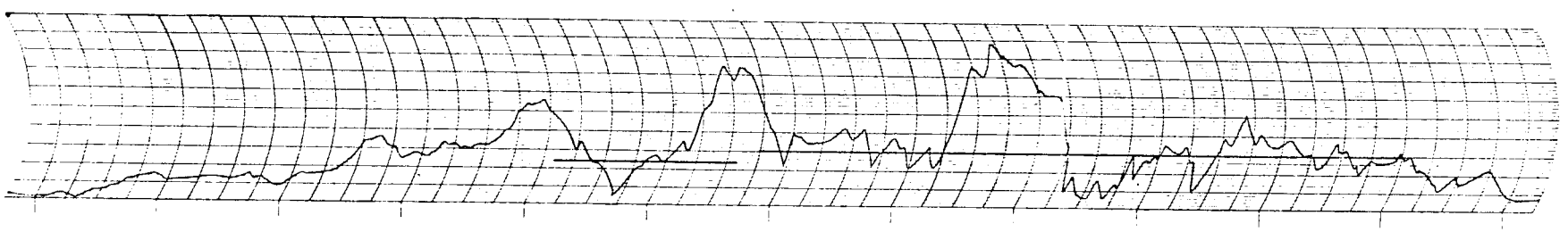

50 Mc/s SIGNAL STRENGTH (AREQUIPA → TRUJILLO)

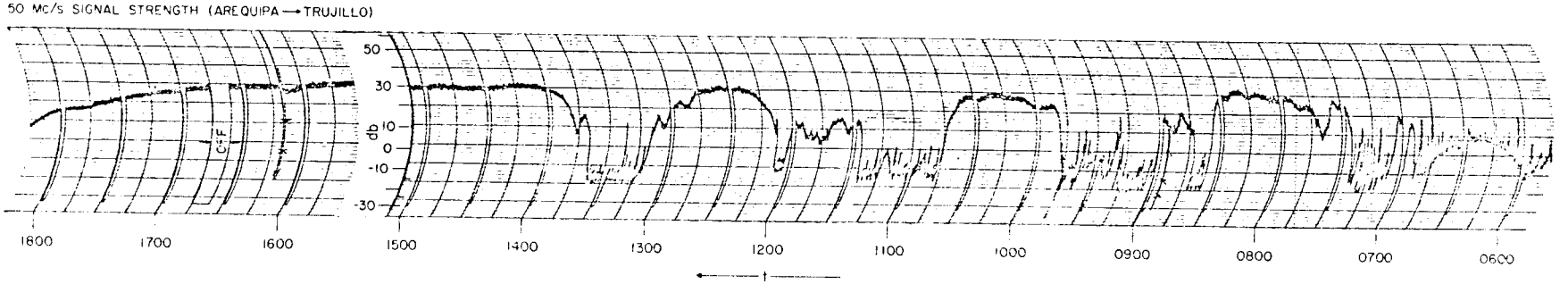

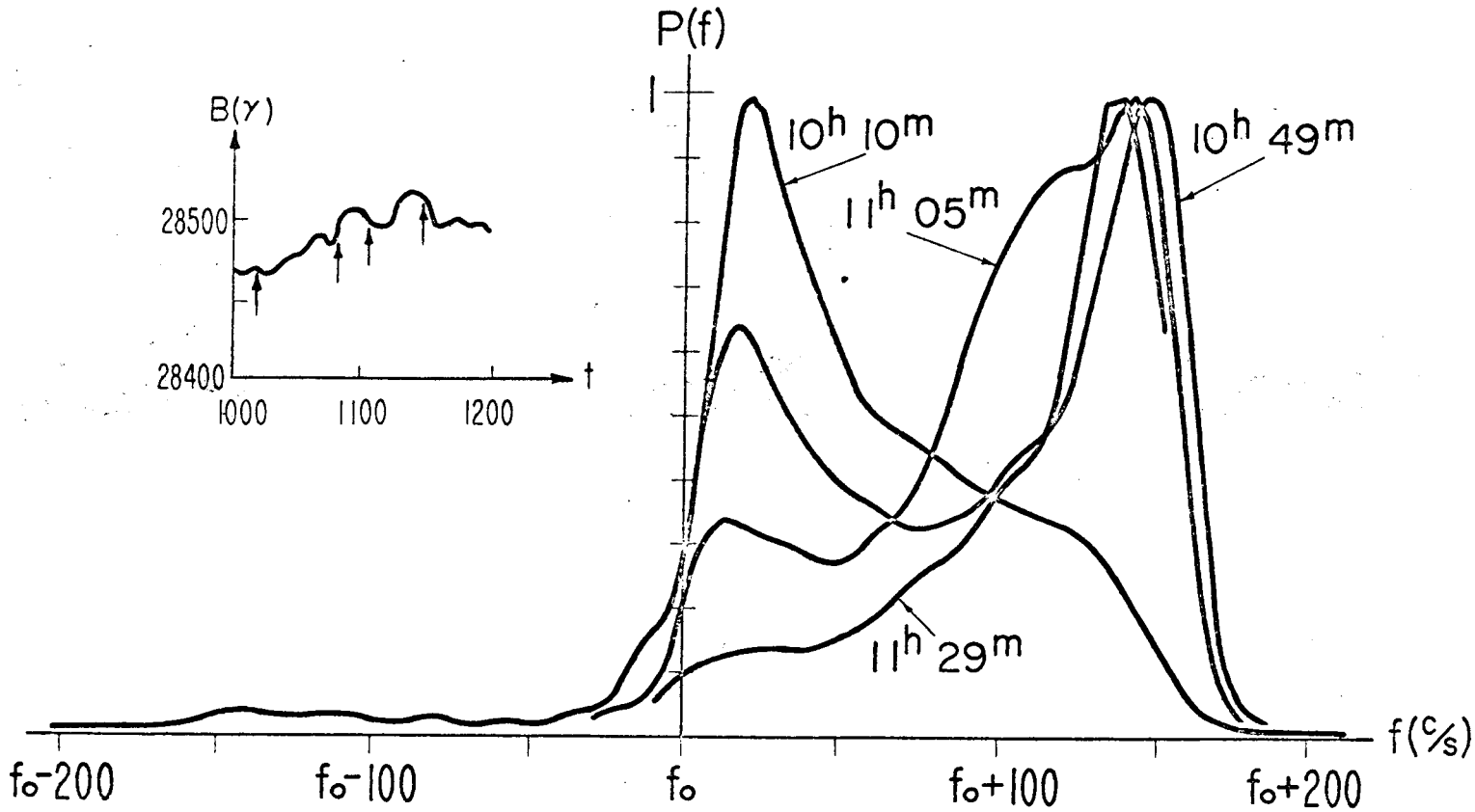

JICAMARCA, PERU
1964 JANUARY 3
75°W. LOCAL TIME
f_o = 49.92 Mc/s
—50° EAST—

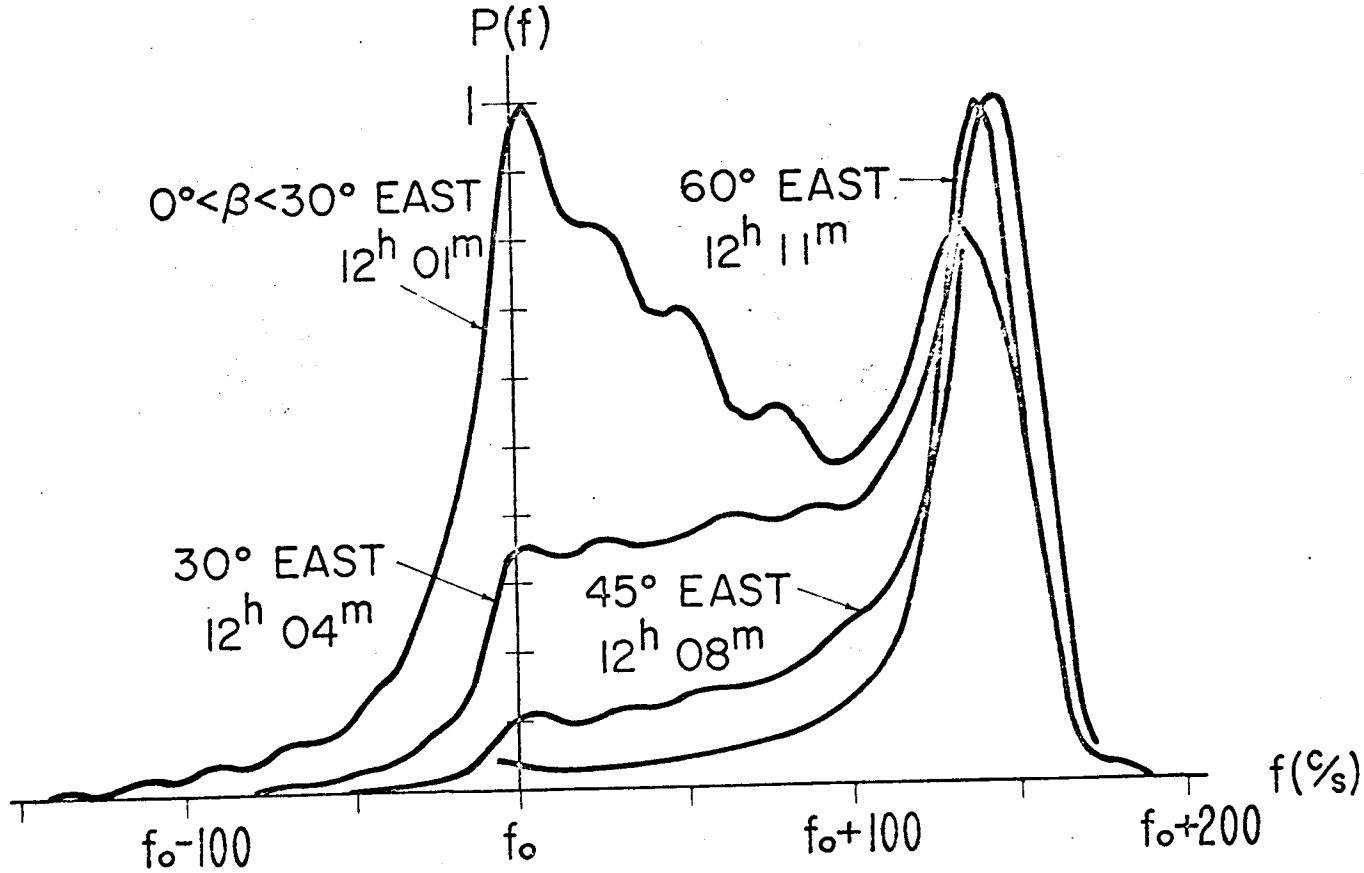

JICAMARCA, PERU
1964 JANUARY 3
75°W. LOCAL TIME
f_o=49.92 Mc/s

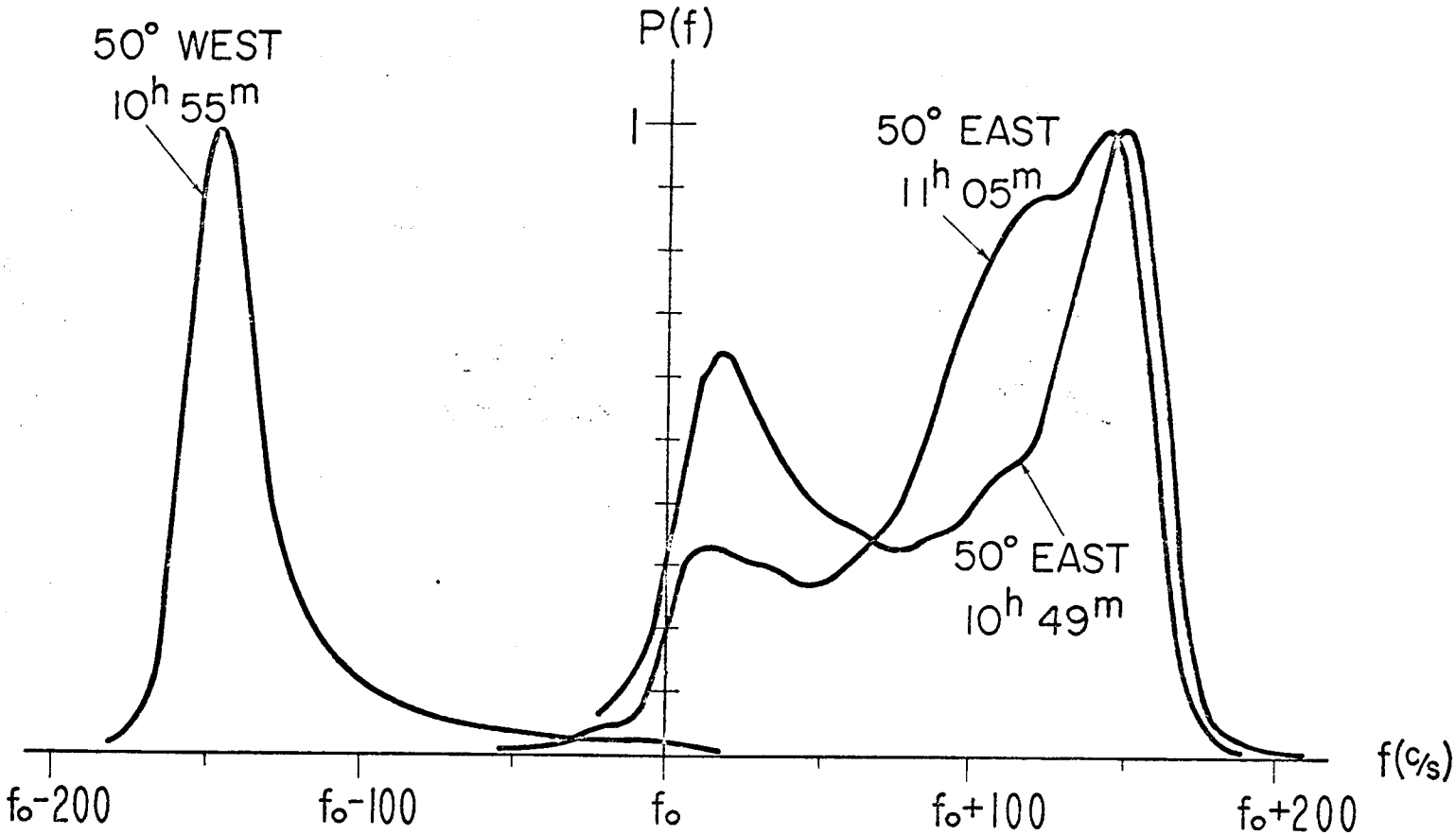

JICAMARCA, PERU
1964 JANUARY 3
75°W. LOCAL TIME
f_o = 49.92 Mc/s

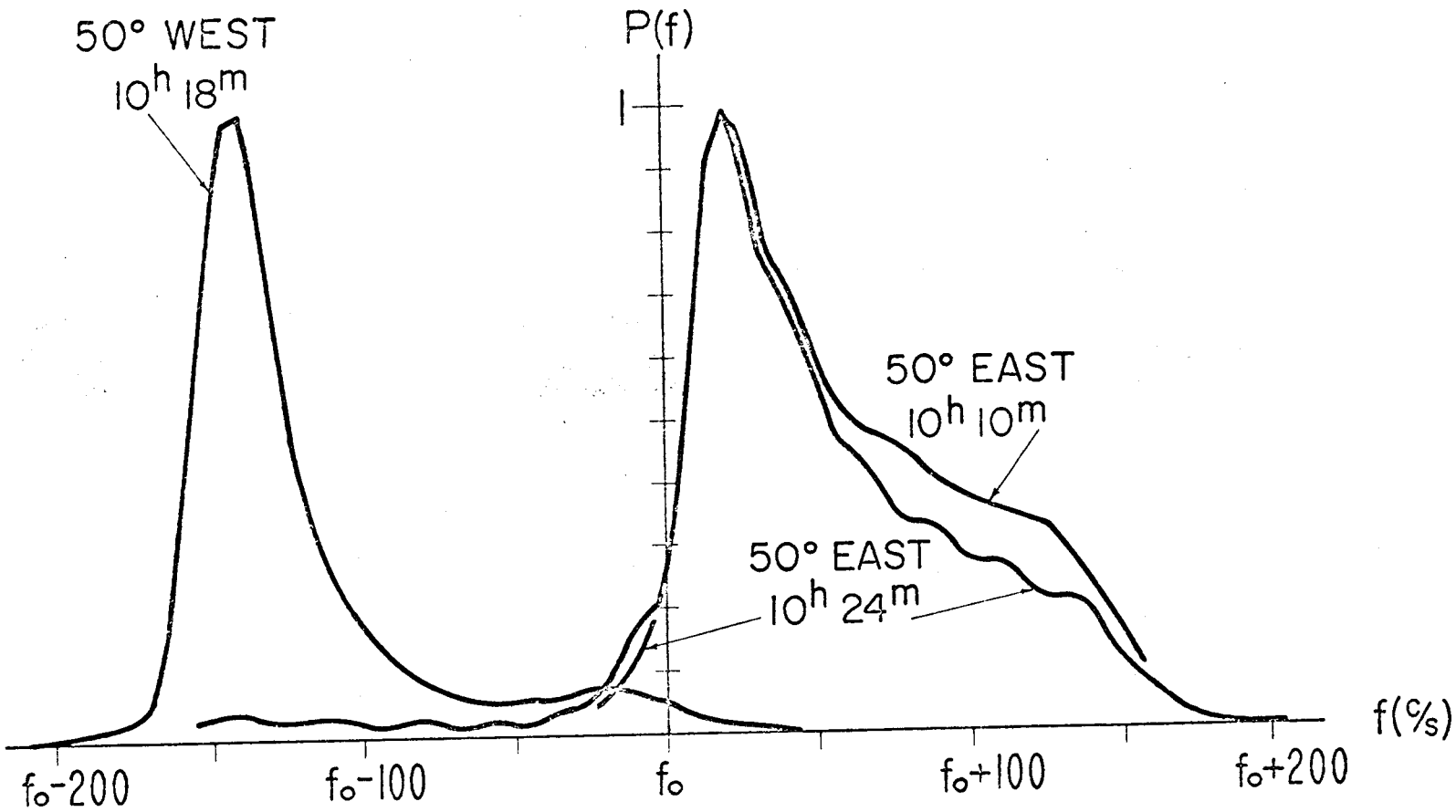

JICAMARCA, PERU
1964 JANUARY 3
75°W. LOCAL TIME
f_o = 49.92 Mc/s